Rotating combustion chambers as a key feature of effective timing of turbine engine working according to Humphrey cycle – CFD analysis

Piotr TARNAWSKI[ID]* and Wiesław OSTAPSKI

Institute of Machine Design Fundamentals, Warsaw University of Technology, Narbutta 84, 02-524 Warsaw, Poland

Abstract. The paper presents a concept of a new turbine engine with the use of rotating isochoric combustion chambers. In contrast to previously analyzed authors' engine concepts, here rotating combustion chambers were used as a valve timing system. As a result, several practical challenges could be overcome. An effective ceramic sealing system could be applied to the rotating combustion chambers. It can assure full tightness regardless of thermal conditions and related deformations. The segment sealing elements working with ceramic counter-surface can work as self-alignment because of the centrifugal force acting on them. The isochoric combustion process, gas expansion, and moment generation were analyzed using the CFD tool (computational fluid dynamics). The investigated engine concept is characterized by big energy efficiency and simple construction. Finally, further improvements in engine performance are discussed.

Key words: pressure gained combustion; Humphrey cycle; turbine engine; CFD analysis; valve timing system; isochoric combustion; engine energy efficiency; sealing system.

1. INTRODUCTION

To improve the energy efficiency of a turbine engine the combustion in a constant volume can be used instead of isobaric combustion. It increases pressure during combustion which has a positive impact. The theoretical thermodynamic Humphrey cycle, which stands behind the idea, is more effective than the Bryton–Joule cycle, based on which contemporary turbine engines operate. For pressure ratio 18 the advantage of the Humphrey cycle is 10% over the Bryton–Joule cycle [1–3].

The creation of a competitive turbine engine working according to the Humphrey cycle requires the implementation of an effective valve timing system [4–7]. Its role is temporary closing and opening of the combustion chambers. Secondly, it must assure the effective conversion of an impulse of high-pressure gas into mechanical energy. Thirdly, it must be integrated with the pressure-tight sealing system of combustion chambers.

A lot of effort was undertaken by the authors to study different valve timing systems [8–12]. It is worth mentioning pulse powered turbine engine concept with implemented rotating valve timing system [11]. The operation of the engine was controlled by a single-component rotating valve timing system. Despite the pulse powering of the engine, the continuity of gas flow in the nozzles was assured. Next, an effective expansion of gas was ensured by the application of different pressure nozzles.

The paper presents a modified engine concept. Instead of rotating nozzles, rotating combustion chambers were implemented. It assured similar controlling of engine operation, but such a configuration has several practical advantages:

- Because of rotating combustion chambers only two sets of injection systems can be used.
- De Laval nozzles are stationary, so they are not loaded by centrifugal force. Only heat and gas pressure affect them, thus they can be made of ceramic materials.
- An effective ceramic sealing system can be applied to the rotating combustion chambers. The segment sealing elements working with ceramic counter-surface can work as self-alignment, because of centrifugal force acting on it. A quite low rotational speed of chambers (1379 rpm) ensures low loading of single-segment element (4 N). This allows a self-aligning seal to be operated without replacement for the required service interval. The proposed system of chamber sealing ensures full tightness regardless of thermal conditions and related deformations.
- Instead of the axial turbine, the radial turbine was implemented. It facilitated a smoother introduction of exhaust gases to the turbine. A decrease in internal losses could be achieved.

In Section 2 a geometry model of the engine is presented, together with the principle of operation and operation parameters. The next section includes details regarding the CFD modeling approach. Section 4 contains CFD results of filling, combustion, and power generation stages. Finally, the most important advantages of the presented engine concept are concluded. Moreover, further possible improvements in engine performance are discussed.

*e-mail: piotrek.tarnawski@gmail.com

Bull. Pol. Acad. Sci. Tech. Sci., vol. 70, no. 5, p. e143100, 2022

1

P. Tarnawski and W. Ostapski

2. GEOMETRY MODEL AND PRINCIPLE OF OPERATION OF PRESENTED ENGINE CONCEPT

The turbine engine concept presented in the paper consists of six rotating combustion chambers ($n = 1379$ rpm), two different stationary de Laval nozzles in a symmetrical arrangement, and a counter-rotating radial turbine ($n = 42000$ rpm) (see Fig. 1 and Fig. 2). The rotating combustion chambers fulfilled the role of engine timing. A constant velocity rotation is required; thus the external driving system should be employed. During the rotation of chambers, a filling, isochoric combustion, and expansion stages are realized. Each stage lasted 0.00725 s. While in one chamber high-pressure gas is being prepared, the second and third chamber is discharging. The gas is expanded firstly by the high-pressure nozzle, and secondly by the low-pressure nozzle. The high-pressure nozzle has a ratio of maximum to minimum cross-section area equal to 3.5 and the low-pressure nozzle has a ratio of maximum to minimum cross-section area equal to 2. A high-velocity gas supplied the turbine producing mechanical work. Full leak thickness was assumed between components being in relative motion.

The intake air was compressed externally by the turbocharger to $p = 1.8$ MPa (first stage) and by the mechanical compressor (second stage). Between the first and second stages of compression cooling of air from $436°C$ to $336°C$ was incorporated.

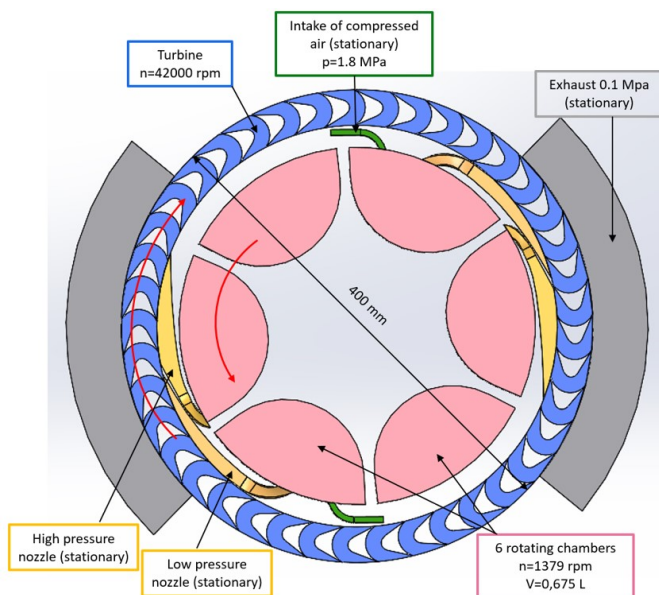The first stage was assumed in a turbocharger (from 0.1 to 0.35 MPa) [12, 13]. An application of a turbocharger facilitated better use of the kinetic energy of exhaust gas. The second stage (from 0.35 to 1.8 MPa) was assumed in a mechanical compressor. A detailed procedure of calculation for air compression presented is in [13].

3. CFD MODELLING APPROACH

3.1. CFD differential equations

A transient set of Navier–Stokes equations, together with a compressible, semi-ideal, energy equation, species transport, and reaction of combustion were resolved [13]. The thermal properties of gas species (specific heat, thermal conductivity, viscosity) were temperature dependent. The commercial ANSYS Fluent software was employed in the analysis.

3.2. Discretization of model

The 3D numerical simulation was performed using mesh consisting of hexahedral elements in the entire domain (see symmetry half of the numerical model in Fig. 3 and Fig. 4). The first element in the vicinity of the walls had a size of 0.25 mm. The mesh was created to assure y plus in the range of 30–300 value. An enhanced wall treatment option [14] was chosen to ensure proper resolution of parameters in the boundary layer.
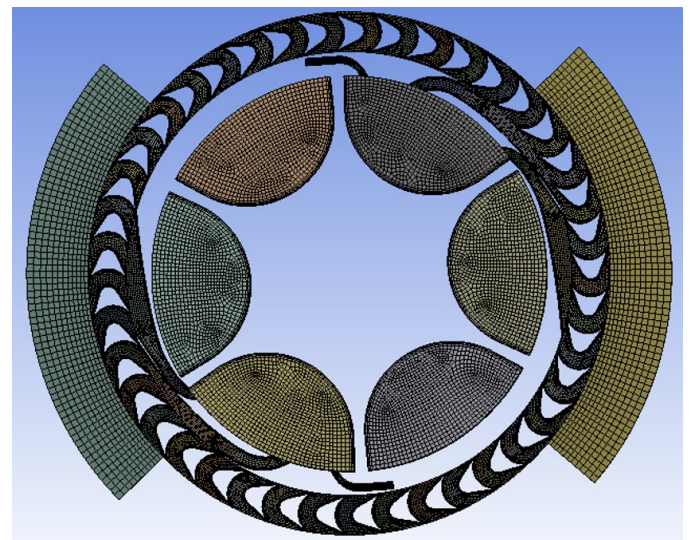

Fig. 1. Geometry model of the turbine engine concept – general view

Fig. 3. Numerical mesh of simulation model of the engine – general view

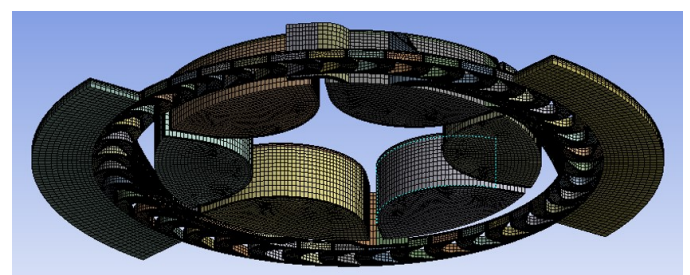**Fig. 2.** Geometry model of the turbine engine concept – top view

Fig. 4. Numerical mesh of simulation model of the engine – top view

3.3. Description of boundary conditions

A constant rotation velocity of $n = 1379$ rpm was prescribed for the combustion chambers and $n = 42000$ rpm for the turbine. *Rotating Mesh Motion* [14] was prescribed for combustion chambers and the turbine. The capability allows to include a real object rotation and to consider the transient interaction of neighboring volume meshes. Between two, in a relative motion adjacent sliding surface, the *Interface* boundary condition was applied [14]. It facilitates exchanging the calculated parameters between different structure meshes. The turbulence was modeled using two different turbulence models, Realizable k-ε and $SSTk$-ω. The *Pressure inlet* with a value of 1.8 MPa was assigned to the intake of compressed air. The *Pressure outlet* with a value of 0.1 MPa was assigned to the gas exhaust. A description of the boundary conditions is shown in Fig. 5.
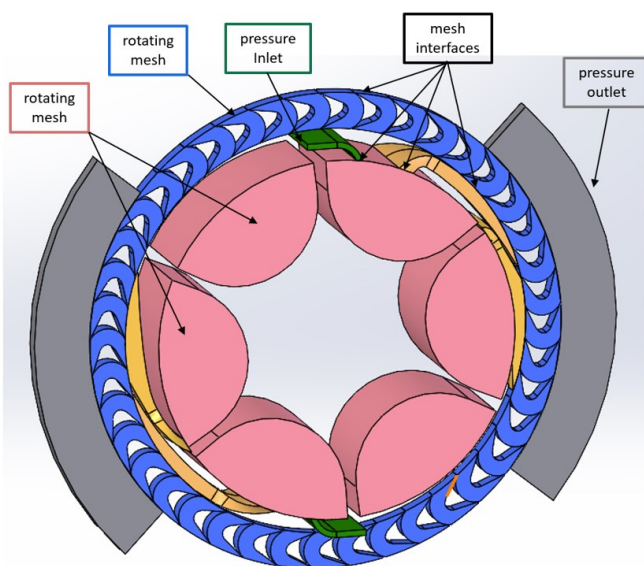

Fig. 6. Simultaneous filling and discharging by low-pressure nozzle

Fig. 5. Description of boundary conditions of the simulation model

Fig. 7. Temperature distribution (left) and oxygen mole fraction distribution (right) during the filling stage (symmetry plane)

4. CFD RESULTS

4.1. Filling of combustion chamber stage

The filling of the combustion chamber with fresh air was realized simultaneously with discharging by the low-pressure nozzle. A properly designed shape of the chamber and an appropriate direction of fresh air inlet ensured effective filling which was crucial in that concept. The filling at compression pressure assured realizing the Humphrey cycle. The fresh, compressed air almost did not mix with exhaust gas (Fig. 6). The fresh air was pushing exhaust gas out of the combustion chamber. The temperature distribution and oxygen mole fraction in the subsequent filling moments in the combustion chamber are presented in Fig. 7. At the end of the filling average oxygen mole fraction was equal to 0.1854.

4.2. Direct injection of fuel and combustion

A classic injection system was used, as in the auto-ignition engine. The injectors were located on opposite sides of the central point of rotating combustion chambers. The decan (C10H22)

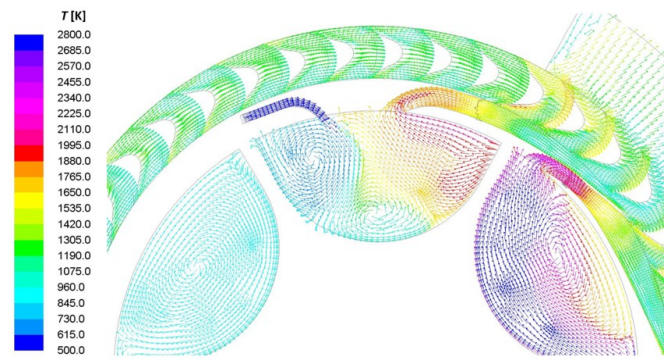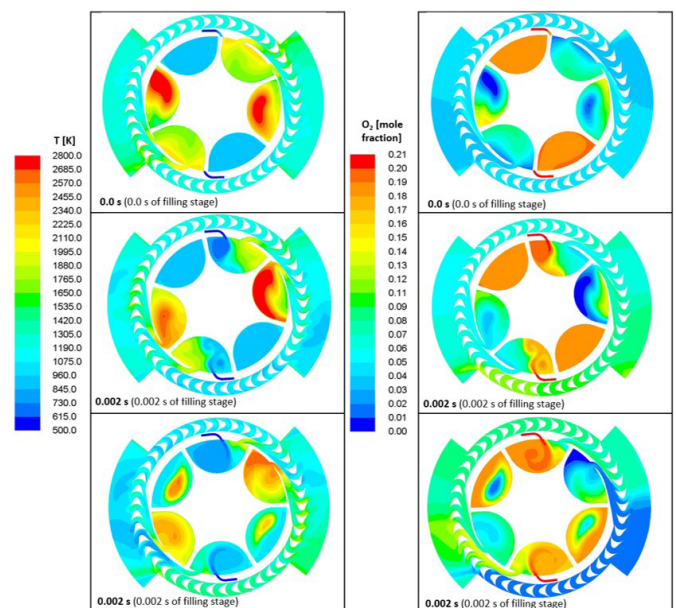was directly injected into combustion chambers at 40 angle degrees (Fig. 8). It allowed effective mixing and evaporation. The spray was simulated using the *Discrete Phase* model [13]. The combustion process was simulated using the *Eddy Dissipation* model [14]. Analytical calculation of the portion of injected fuel was based on simulation results. The amount of fresh gas that filled the combustion chamber was equal to 0.00395 kg and the final averaged oxygen mole fraction was equal to 0.1854. Assuming excess air coefficient $\lambda = 1.6$, the mass portion of the injected fuel was equal to 0.000184 kg. A detailed procedure of calculation for fuel demand can be found in [13]. The chemical energy consumed for a single combustion cycle was equal to 8.208 kJ. The combustion process continued according to the chemical reaction (1):

$$C_{10}H_{22} + 15.5O_2 = 10CO_2 + 11H_2O. \qquad (1)$$
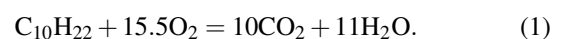
The temperature was increasing as the combustion process continued. The maximum temperature at the end combustion stage reached 2800 K. The distribution of temperature at char-
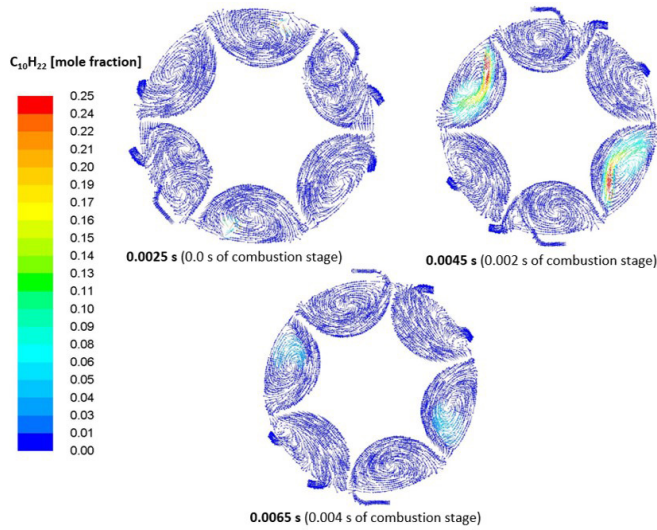
Bull. Pol. Acad. Sci. Tech. Sci., vol. 70, no. 5, p. e143100, 2022

3

Fig. 8. Distribution of fuel mole fraction during the combustion

acteristic periods of the combustion stage is presented in Fig. 9. The walls of the combustion chambers and the walls of nozzles were cooled. A constant wall temperature of 1573 K was set in the simulation model. For the state of the art of contemporary ceramic materials, it seems a reasonable assumption [15].
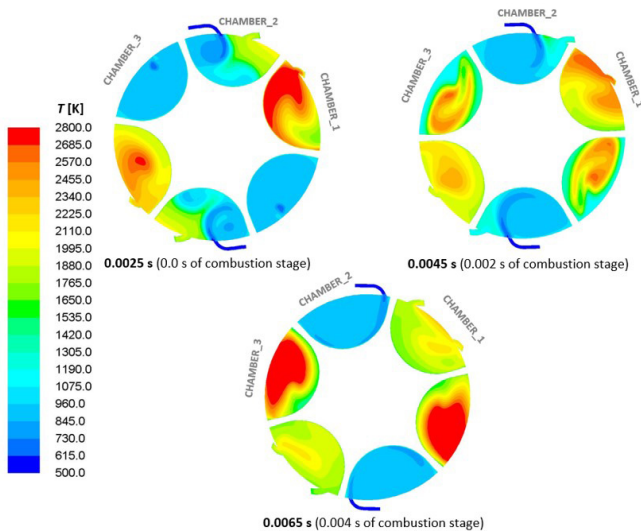

Fig. 9. Distribution of temperature during the isochoric combustion

The pressure and temperature of the gas in the combustion chamber and nozzles was changing according to different stages of the engine cycle (Fig. 10 and Fig. 11). The lowest value of 1.5 MPa was at the beginning of the filling. The filling proceeded almost isobarically. The maximum value reached 5.2 MPa at the end of combustion. The increase in pressure is similar to that obtained in [16] and [17]. The pressure in the high-pressure nozzle has changed from 1.55 to 4.75 to MPa. The pressure in the low-pressure nozzle has changed from 1.3 to 2.75 MPa. It is worth noticing here the undisputed advantage of the engine working according to the Humphrey cycle. Namely, the gas is expanded from higher averaged pressure than the

pressure of compression. In a classical turbine engine, working according to the Bryton–Joule cycle, the expansion takes place from the pressure of compression. Higher stagnant pressure assures higher kinetic energy of gas after expansion.

The lowest temperature 950 K was at the end of filling. The maximum average temperature of 2360 K was at the end of the combustion.
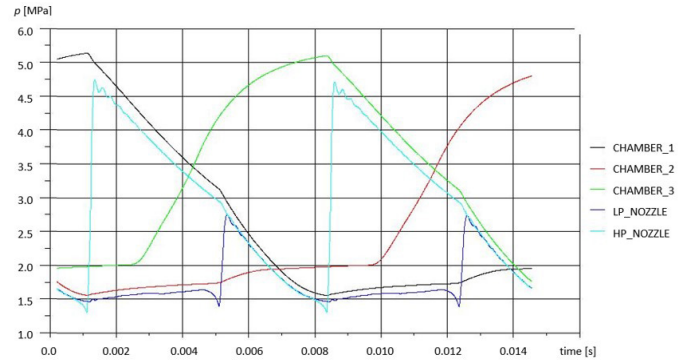

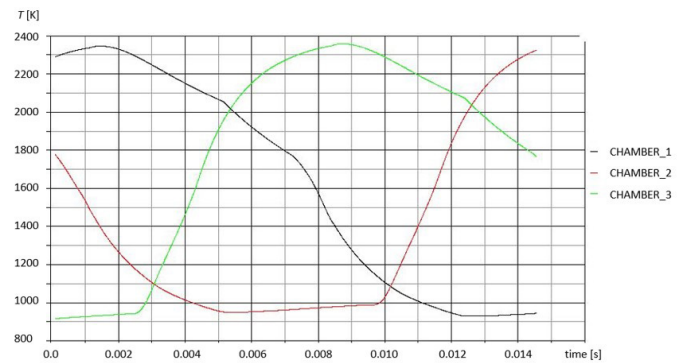**Fig. 10.** Change of pressure during the engine cycle

Fig. 11. Change of temperature during the engine cycle

4.3. Torque and work generation

A high-pressure gas was expanding which caused the acceleration in de Laval nozzles. The high velocity of gas (ranging between 2 and 3 Mach) was supplying the turbine. As a result, a mechanical moment was generated. The Mach number distribution in different moments of discharging stage is presented in Fig. 12.

The expansion of gas to low pressure (0.1 MPa) in de Laval nozzles caused a significant decrease in the temperature (Fig. 13). The temperature in the vicinity of blades ranges from 950 K to 1400 K (Fig. 14). Such a low temperature excludes the need for the cooling of turbine blades. The supersonic shape of the turbine blade assured appropriate pressure distribution on both sides of the blade [18].

The torque generated in the turbine for the *Realizablek-ε* turbulence model changed from −68 to −170 Nm (Fig. 15). The lowest value was obtained right before the opening of the chamber with the nozzles. An arithmetically averaged torque amounted to 127.6 Nm (for the symmetrical half of the engine). The torque generated in the turbine for the *SST k-ω* turbulence

4

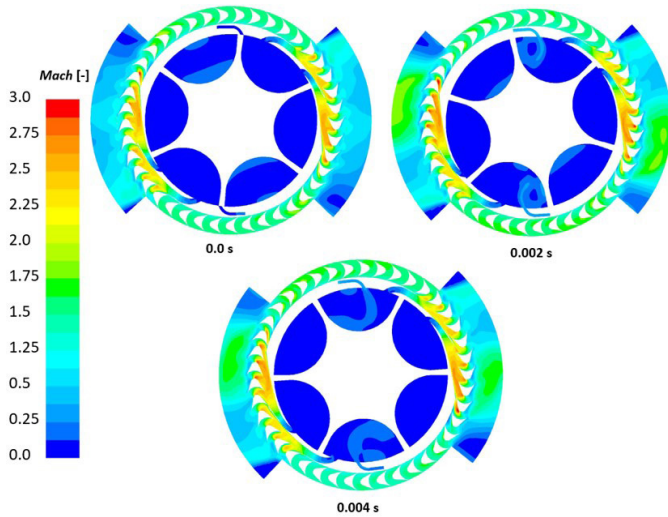*Bull. Pol. Acad. Sci. Tech. Sci.*, vol. 70, no. 5, e143100, 2022

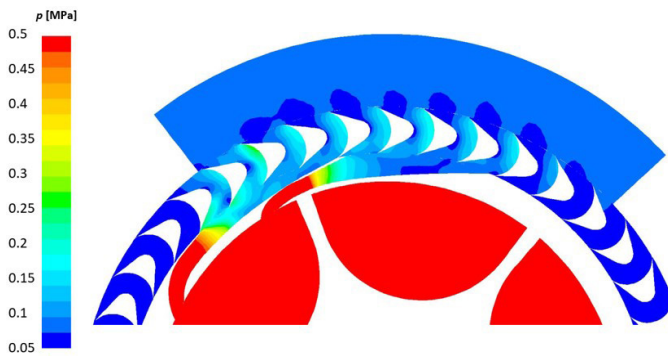**Fig. 12.** Distribution of Mach number (symmetry plane)

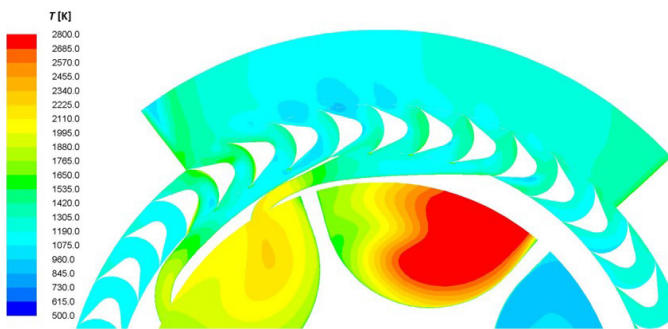**Fig. 13.** Distribution of pressure in nozzles and in the area of blades (symmetry plane)

Fig. 14. Distribution of temperature in the area of blades (symmetry plane)

Fig. 15. Torque generated in turbine for 2 discharging engine cycles – *Realizable k-ε* model
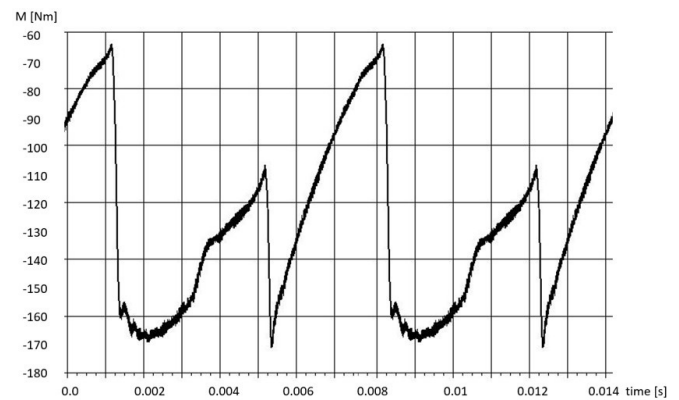
Fig. 16. Torque generated in turbine for 2 discharging engine cycles – *SST k-ω* model

where: L_e [kJ] – effective work, M_{avg} [Nm] – averaged moment, n [rpm] – rotational velocity, t_{cycle} [s] – cycle time of discharging, $9549 = 60/(2 \cdot \pi \cdot 1000)$ – dimensionless unit converter, $\eta_m = 0.95$ – mechanical efficiency of the turbine.

Using equation (3) the effective power of the engine reached 789.8 kW:

$$N_e = \frac{L_e}{t_{cycle}} . \qquad (3)$$

Considering injected chemical energy of fuel, the engine effective efficiency reached 0.3584. It was calculated from equation (4):

$$\eta_E = \frac{L_e}{E_{chem}} , \qquad (4)$$

where: η_E [–] – engine energy efficiency.

The final calculated parameter was specific fuel consumption. Based on equation (5), it amounted to 231.35 g/kWh:

$$g = \frac{m_{C_{10}H_{22}} \cdot 1000 \cdot 3600}{t_{cycle} \cdot N_e} , \qquad (5)$$

where: g [g/kWh] – specific fuel consumption.

A summary of calculated parameters of the presented engine concept is presented in Table 1.

model was very similar, which gives credibility to the obtained results. The average value amounted to 127.5 Nm (Fig. 16).

Effective work produced in the turbine for one discharging cycle (0.00725 s) was equal to 5.884 kJ. It was determined from equation (2). The mechanical efficiency of the turbine was assumed 0.95:

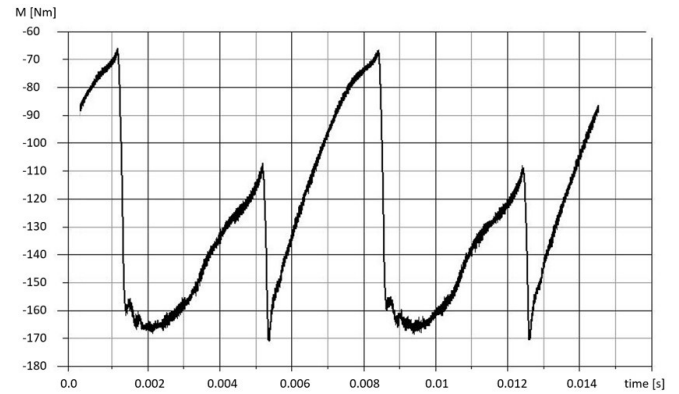$$L_e = \frac{M_{avg} \cdot n \cdot t_{cycle}}{9549} \eta_m , \qquad (2)$$

Bull. Pol. Acad. Sci. Tech. Sci., vol. 70, no. 5, p. e143100, 2022

5

P. Tarnawski and W. Ostapski

Table 1
Calculation of important parameters of the presented engine concept

Parameter description	Value
The chemical energy of fuel	$E_{\text{chem}} = 16.417$ kJ
Effective kinetic energy demand for turbocharger ($\eta_{eC} = \eta_{iC} \cdot \eta_T = 0.85 \cdot 0.85 = 0.7225$)	$L_{eC\_\text{turbospr}} = 1.409$ kJ
Effective demand for work in mechanical compressor ($\eta_{eS} = \eta_{iS} \cdot \eta_{mS} = 0.85 \cdot 0.97 = 0.8245$)	$L_{eC\_\text{mech}} = 1.914$ kJ
Effective work of turbine	$L_{eT} = [(255.2 \text{ Nm} \cdot 42000 \text{ rpm} \cdot 0.00725 \text{ s})/9549] \cdot 0.95 = 7.731$ kJ
The kinetic energy of gas behind the turbine	$E_{k\_T} = 1.476$ kJ
Effective engine work	$L_e = 7.731 - 1.409 - 1.914 + 1.476 = 5.884$ kJ
Effective engine power	$N_e = 5.884/0.00725s = 789.8$ kW
The effective energy efficiency of the engine concept	$\eta_E = 5.884/16.417 = \mathbf{0.3584}$
Specific fuel consumption	$g = 2 \cdot 0.000184 \cdot 1000 \cdot 3600/(0.00725 \cdot 789.8) = 231.36$ g/kWh

5. CONCLUSIONS

The paper presents a CFD analysis of mechanical power generation and effective energy efficiency evaluation for the new turbine engine concept. It is a promising design as it is characterized by the big effective energy efficiency of 35.8% and low 231.36 g/kWh specific fuel consumption while maintaining small engine dimensions and power.

It is worth comparing the results to the similar power turboshaft classical turbine engines existing on the market. The Pratt & Whitney Canada PT6C-67C (820 kW) has an effective energy efficiency equal to 27.5% [19]. The second example is the MTU Turbomeca Rolls-Royce MTR390 (958 kW), which has an effective energy efficiency equal to 29.3% [19]. However, the comparison of engine parameters should be treated with some caution. The presented efficiencies of engines of well-known companies are brake parameters measured for real engines. The presented parameters of the turbine engine concept with rotating combustion chambers are the result of computer simulation. Because of CFD modeling simplifications for calculated parameters, an error margin is possible.

In contrast to previously analyzed authors' engine concepts, here rotating combustion chambers were used as a valve timing system. As a result, several practical challenges could be overcome:
- Only two sets of injection systems could be used.
- De Laval nozzles are stationary, so they are not loaded by centrifugal force. Only heat and gas pressure affect them, thus they can be made of ceramic materials.
- An effective ceramic sealing system could be applied to the rotating combustion chambers. The segment sealing elements working with ceramic counter-surface can work as self-alignment because of the centrifugal force acting on them. The proposed system of seals ensures full chamber tightness, regardless of thermal conditions and related deformations.

A significant advantage of the presented engine concept is its simple and compact design. What stands behind it, is possible lower production costs, compared to similar engines with isobaric combustion.

Further improvement of efficiency of engine concept should be focused on the investigation of the influence of combustion chamber volume and length of expansion stage. However, an increase in the volume of the chamber in the current arrangement must decrease its rotation velocity. In turn, a decrease in the rotation velocity of chambers causes a higher generation of losses during the opening of the chamber. Thus, another arrangement of chambers should be proposed. The next improvement could be achieved by the elimination of losses concerned with partial turbine load [9]. The power of the engine had to increase twice or three times, because of supplying the turbine on its entire circumference. Finally, to assure better engine performance, further improvement of the filling stage should be undertaken. The higher the oxygen content after filling, the better. The higher the oxygen content in the combustion chamber, the higher the effective efficiency of the engine. The possibility of a further increase in engine efficiency makes the concept very promising. It is believed that the presented turbine engine concept should develop based on the assumption of rotating combustion chambers.

REFERENCES

[1] P. Tarnawski, "Analytical performance evaluation of Humphrey for turbine engine application," *Mach. Dyn. Res.*, vol. 41, no 3, 27–37, 2017.

[2] K. Kamiuto, "Comparison of basic gas cycles under the restriction of constant heat addition," *Appl. Energy*, vol.83, no. 6, 2006, pp. 583–593, 2005, doi: 10.1016/j.apenergy.2005.05.008.

[3] P. Stathopoulos, "Comprehensive thermodynamic analysis of the Humphrey cycle for gas turbines with pressure gain combustion," *Energies*, 11, p. 3521, 2018, doi: 10.3390/en11123521.

[4] C. Brophy and G. Roy, "Benefits and challenges of pressure-gain combustion systems for gas turbines," *Mech. Eng.*, vol. 131, no. 3, pp. 54–55, 2009, doi: 10.1115/1.2009-MAR-8.

6

Bull. Pol. Acad. Sci. Tech. Sci., vol. 70, no. 5, p. e143100, 2022

Rotating combustion chambers as a key feature of effective timing of turbine engine working according to Humphrey cycle – CFD analysis

[5] F. Walraven, "Operational Behavior of a Pressure Wave Machine with Constant Volume Combustion," *ABB Technical Report* CHCRC 94–10, 1994.

[6] K. Kurec, J. Piechna, and K. Gumowski, "Investigations on unsteady flow within a stationary passage of a pressure wave exchanger by means of PIV measurements and CFD calculations," *Appl. Therm. Eng.*, vol. 112, no. 5 , pp. 610–620, 2017, doi: 10.1016/j.applthermaleng.2016.10.142.

[7] P. Akbari and M.R. Nalim, "Review of recent developments in wave rotor combustion technology," *J. Propul. Power*, vol. 25, no. 4, pp. 833–844, 2009, doi: 10.2514/1.34081.

[8] P. Tarnawski and W. Ostapski, "Pulse powered turbine engine concept – Numerical analysis of influence of different valve timing concepts on thermodynamic performance," *Bull. Pol. Acad. Sci. Tech. Sci.*, vol. 66, no. 3, pp. 373–382, 2018, doi: 10.24425/123444.

[9] P. Tarnawski, "Pulse powered turbine engine concept," Ph.D. dissertation, Poland: Warsaw University of Technology, Warsaw, 2018.

[10] P. Tarnawski, and W. Ostapski, "Pulse powered turbine engine concept implementing rotating valve timing system: Numerical CFD analysis," *J. Aerosp. Eng.*, vol. 32, no. 3, p. 04019017, 2018.

[11] P. Tarnawski and W. Ostapski, "Turbine engine concept realizing Humphrey cycle," in *Materials, Technologies, Constructions – Constructions and Design*, vol. 4. A. Mazurkow, Ed., Poland: Rzeszow University of Technology, 2019, pp 23–43.

[12] Turbo Tech 103 Expert, "Compressor Mapping", Garret Advancing Motion. [Online]. Available: https://www.garrett motion.com/wp-content/uploads/ 2019/10/GAM_Turbo-Tech-103_Expert-1.pdf. [Accessed:10 Dec. 2020].

[13] P. Tarnawski and W. Ostapski, "A concept of a pulse-powered turbine engine with application of self-acting displacement valves- 3D numerical analysis," *SAE Int. J. Engines*, vol. 14, no. 3, pp. 419–437, 2021, doi: 10.4271/03-14-03-0025.

[14] ANSYS® Academic Associate CFD, *ANSYS Fluent User Guide, Release 18.1.* Canonsburg, PA,USA, ANSYS Inc., 2016.

[15] D. Derlukiewicz, "Method of modeling of thermo-elastic phenomena in layered ceramic coatings". Ph.D. dissertation, Poland: Wroclaw University of Technology, Wroclaw, 2006.

[16] J. Li, E. Gong, W. Li, K. Zhang, and L. Yuan, "Investigation on combustion properties in simplified wave rotor constant volume combustor," *21st AIAA International Space Planes and Hypersonics Technologies Conference*, 2017, doi: 10.2514/6.2017-2384.

[17] L. Labarrere, T. Poinsot, A. Dauptain, F. Duchaine, M. Bellenoue, and B. Boust, "Experimental and numerical study of cyclic variations in a constant volume combustion chamber," *Combust. Flame*, vol. 172, pp. 49–61, 2016, doi: 10.1016/j.combustflame.2016.06.027.

[18] H. Kato, H. Mashiko, K. Funazaki, and J. Takida, "Multiobjective aerodynamic optimization of a supersonic turbine for higher efficiency and smaller load fluctuation," *10th World Congress on Structural and Multidisciplinary Optimization*, 2013.

[19] Gas Turbine Engines, "Aviation week and space technology," Geocities. [Online]. Available: http://www.geocities.jp/nomonomo2007/AircraftDatabase/AWdata/AviationWeekPages/GTEnginesAWJan2008.pdf. [Accessed: 28 Jan. 2018].